# A Modified Neighborhood Similar Pixel Interpolator Approach for Removing Thick Clouds in Landsat Images

Xiaolin Zhu, Feng Gao, Desheng Liu, and Jin Chen

***Abstract*—Thick-cloud contamination is a common problem in Landsat images, which limits their utilities in various land surface studies. This letter presents a new method for removing thick clouds based on a modified neighborhood similar pixel interpolator (NSPI) approach that was originally developed for filling gaps due to the Landsat ETM+ Scan Line Corrector (SLC)-off problem. The performance of the proposed method was evaluated with both simulated and real cloudy images and compared with that of a contextual multiple linear prediction (CMLP) method. The results show that the modified NSPI approach can greatly reduce the edge effects by CMLP. The reflectance restored by the modified NSPI approach is more accurate than that by CMLP, especially when the cloud-free auxiliary and cloudy images are acquired from different seasons and have different spectral characteristics.**

***Index Terms*—Cloud removal, image processing, image restoration, Landsat.**

## I. Introduction

LANDSAT images provide the longest satellite observations of the Earth's land surface that are crucial to a wide range of remote sensing studies. However, due to the nature of optical sensors and the relative long revisit cycle, Landsat images are highly affected by thick-cloud contamination [1], which presents a serious obstacle in their applications, especially in monitoring land surface dynamics. Therefore, removing thick clouds in Landsat images is necessary for improving their quality and availability.

Manuscript received January 21, 2011; revised September 19, 2011; accepted October 17, 2011. Date of publication December 5, 2011; date of current version March 7, 2012. This work was supported in part by the Project 863 of China under Grant 2009AA12004, by the National Science Foundation under Award 1010314, by the State Key Laboratory of Earth Surface Processes and Resource Ecology, and by the International S&T Cooperation Program under Grant 2010DFB10030.

X. Zhu was with the State Key Laboratory of Earth Surface Processes and Resource Ecology, Beijing Normal University, Beijing 100875, China. He is now with the Department of Geography, The Ohio State University, Columbus, OH 43210 USA.

F. Gao is with the Hydrology and Remote Sensing Laboratory, Agricultural Research Service, U. S. Department of Agriculture, Beltsville, MD 20705 USA.

D. Liu is with the Department of Geography and the Department of Statistics, The Ohio State University, Columbus, OH 43210 USA (e-mail: liu.738@osu.edu).

J. Chen is with the State Key Laboratory of Earth Surface Processes and Resource Ecology, Beijing Normal University, Beijing 100875, China.

Color versions of one or more of the figures in this paper are available online at http://ieeexplore.ieee.org.

Digital Object Identifier 10.1109/LGRS.2011.2173290

In general, methods for removing thick clouds require cloud-free images as auxiliary images to restore spectral information blocked by clouds [2]–[5]. Helmer and Ruefenacht proposed a strategy using regression trees and histogram matching for producing cloud-free imagery [2]. Meng *et al.* developed a closest spectral fit (CSF) method to replace spectral values of cloudy pixels by cloud-free pixels using location-based one-to-one correspondence and spectral-based closest fit [3]. Melgani introduced a contextual multiple linear prediction (CMLP) process for reconstructing spectral values of cloudy area in Landsat Enhanced Thematic Mapper plus (ETM+) images, and it was proved to be better than other existing methods [4]. The CMLP approach was then improved by making use of spatial and spectral correlations [5]. One limitation of these existing methods is that the cloud-free image should be acquired at a date as close as possible to the cloudy image to ensure similar spectral characteristics [2], [3], which is often hard to meet in practice. In addition, the spatial continuity of ground features may not be preserved in the restored image with these methods [2]–[5]. That is, the predicted values on the boundary of clouds are somewhat different from the neighboring pixels outside the clouds, resulting in a visual disruption between the clouds and their neighborhood (referred to as edge effects).

Recently, a neighborhood similar pixel interpolator (NSPI) approach was developed to fill gaps in Landsat ETM+ Scan Line Corrector (SLC)-off images [6]. This approach can keep the spatial continuity of filled images even using the auxiliary image with a long time interval [6]. Similar idea could be applied to remove thick clouds in Landsat images. However, as spatial patterns of clouds are very different from those of the SLC-off gaps, modifications to the NSPI approach are needed for thick-cloud removal. In this letter, we introduce a modified NSPI approach for removing thick clouds in Landsat images. The performance of the approach is evaluated with both simulated and real clouds in Landsat images.

## II. Methodology

### A. NSPI Approach

The NSPI approach uses a weighted linear model to predict the spectral value of a target pixel (i.e., an unscanned pixel) from its neighboring similar pixels [6]. The similar pixels have similar spectral characteristics with the target pixel and are assumed to have a similar change trend to the target pixel.

Two initial predictions using the spectro-spatial and spectro-temporal information can be calculated according to (1) and (2), respectively

$$L_1(x,y,t_2,b) = \sum_{i=1}^{N} W_i \times L(x_i,y_i,t_2,b) \quad (1)$$

$$L_2(x,y,t_2,b) = L(x,y,t_1,b) + \sum_{i=1}^{N} W_i (L(x_i,y_i,t_2,b) - L(x_i,y_i,t_1,b)) \quad (2)$$

where $L(x_i, y_i, t_1, b)$ is the value of the $i$th similar pixel in band $b$ at date $t_1$, $L(x_i, y_i, t_2, b)$ is with the same definition but at date $t_2$, $L_1(x, y, t_2, b)$ is the prediction of the target pixel based on the spectro-spatial information, $L_2(x, y, t_2, b)$ is the prediction based on the spectro-temporal information, $N$ is the number of similar pixels, and $W_i$ is the weight of the $i$th similar pixel.

NSPI employs an adaptive moving window and a threshold to identify the similar pixels. The weights $W_i$ are calculated from the product of a spatial distance $(D_i)$ and a spectral distance $(RMSD_i)$, where $D_i$ is the Euclidean distance between the $i$th similar pixel and the target pixel and $RMSD_i$ can be calculated as

$$RMSD_i = \sqrt{\frac{\sum_{b=1}^{K} (L(x_i, y_i, t_1, b) - L(x, y, t_1, b))^2}{K}} \quad (3)$$

where $K$ is the number of bands. Last, a weighted combination of the two initial predictions is used to compute the final prediction. The weights ($T_1$ and $T_2$) are determined by the extent of the landscape homogeneity and the extent of spectral change between input and target images within the moving window [6]. Therefore, the final prediction can be obtained

$$L(x, y, t_2, b) = T_1 \times L_1(x, y, t_2, b) + T_2 \times L_2(x, y, t_2, b). \quad (4)$$

### B. Improvements for Cloud Removal

Following the idea of NSPI, it is reasonable to assume that neighboring pixels around cloudy pixels have a similar change trend of reflectance to cloudy pixels if their spectral characteristics are similar. Thus, it is possible to employ an NSPI approach to restore the spectral values of cloudy pixels using the information of the neighboring similar pixels. However, clouds are often randomly shaped clusters, mostly with a much larger size than the narrow wedge-shaped SLC-off gaps. To account for this difference of spatial pattern, modifications to the NSPI approach are needed to make it appropriate for thick-cloud removal.

Fig. 1 shows a flowchart of the modified NSPI approach. It requires an auxiliary image acquired at date $t_1$, which is cloud free for the cloudy parts of the cloudy image acquired at date $t_2$. The detailed descriptions for the steps that are different from the original NSPI approach are given as follows.

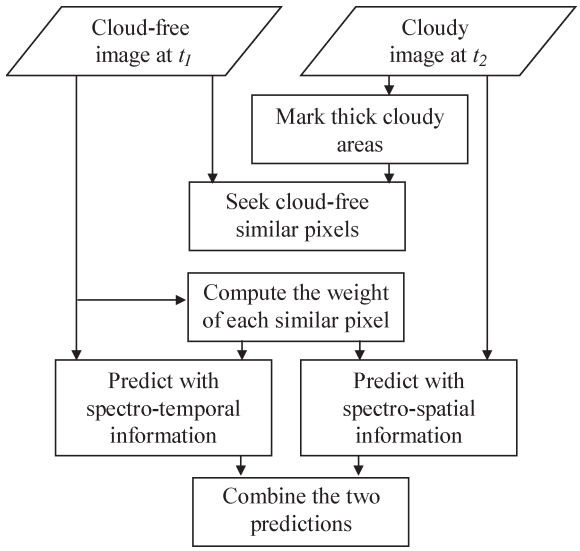


Fig. 1. Flowchart of the modified NSPI approach for thick-cloud removal.

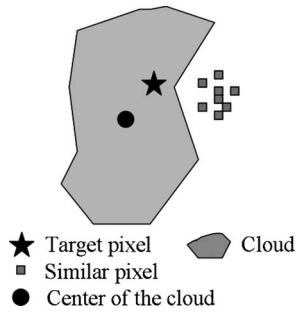


Fig. 2. Schematic diagram of the similar pixel selection.

First, a cloud mask is required beforehand for this algorithm. In general, thick clouds are brighter in visible bands and colder in thermal bands than the land surface. These spectral characteristics can be used to generate cloud masks [7]. In this letter, we used the known cloud masks for simulated thick clouds and visually interpreted cloud masks for real thick clouds, given that cloud detection is not the focus of this letter.

Second, the adaptive window originally used to search similar pixels for the SLC-off gap filling may not be appropriate for removing thick clouds because a large window is needed to cover large clouds. Accordingly, a modified procedure was used to search for the spectrally similar pixels around the clouds (Fig. 2). In detail, from the cloud-free image, $N$ spatially nearest pixels outside the clouds which satisfy the spectral similarity criteria [6], [8] were selected as similar pixels.

Third, in the gap-filling process, similar pixels are very close to the gap pixels because gaps are very narrow, so the range of spatial distances $D_i$ is comparable to the range of spectral distances $RMSD_i$. However, in the cloud-removal process, the distance between a cloudy pixel and its similar pixels may vary greatly, which could make the range of spatial distances incomparable with that of spectral distances. Therefore, spatial

distances ($D_i$) and spectral distances ($RMSD_i$) were both normalized and rescaled as follows:

$$D_i^* = \frac{D_i - D_{\min}}{D_{\max} - D_{\min}} + 1 \tag{5}$$

$$RMSD_i^* = \frac{RMSD_i - RMSD_{\min}}{RMSD_{\max} - RMSD_{\min}} + 1 \tag{6}$$

where the subscripts "min" and "max" represent the minimum and maximum values, respectively; value 1 is an offset to define the relative importance of the two distances. The two distance measures were then combined to calculate the weights in (1) and (2)

$$W_i = \left(1/\left(D_i^* \times RMSD_i^*\right)\right) / \sum_{j=1}^{N} \left(1/\left(D_j^* \times RMSD_j^*\right)\right). \tag{7}$$

Last, the weights ($T_1$ and $T_2$) used to combine the two initial predictions in (4) may not be appropriate for cloud removal because it is hard to assess the local spatial homogeneity and the extent of change for a whole cloud patch whose size is usually larger than the SLC-off gaps. Hence, the weights for the two initial predictions were modified for thick-cloud removal. Specifically, if the target pixel is near the cloud boundary, the first prediction should be given a larger weight because it is based on the spectro-spatial information from the same image and can keep the spatial continuity better and reduce edge effects. If the target pixel is located near the cloud center, the second prediction based on the spectro-temporal information is more reliable because the spectro-spatial information becomes less useful around the cloud center where a target pixel is farther to its similar pixels. Therefore, the weights combining the two predictions can be determined by the relative spatial distances from the target pixel to its similar pixels and to the cloud center. The cloud center is computed by averaging the coordinates of all cloudy pixels (e.g., the circle in Fig. 2). Finally, the value of the target pixel can be predicted as

$$L(x,y,t_2,b) = (L_1(x,y,t_2,b)/r_1 + L_2(x,y,t_2,b)/r_2)/(1/r_1 + 1/r_2) \tag{8}$$

where $r_1$ represents the average spatial distance between the target pixel and its similar pixels and $r_2$ represents the spatial distance between the target pixel and the cloud center.

## III. Algorithm Tests

### A. Experimental Design

We tested the modified NSPI approach using simulated and real cloudy images. Three Landsat 7 ETM+ images acquired on January 25, July 4, and August 5 of 2002 in central Virginia (37° N, 77° W) were obtained from the USGS and atmospherically corrected using the Landsat Ecosystem Disturbance Adaptive Processing System [9]. All three images were then coregistered and orthorectified using the Automated Registration and Orthorectification Package [10]. Two subset scenes (500 × 500 pixels) that correspond to a heterogeneous landscape [Fig. 3(a)] and a homogeneous landscape [Fig. 3(c)] were extracted from the Landsat images for simulation analysis.

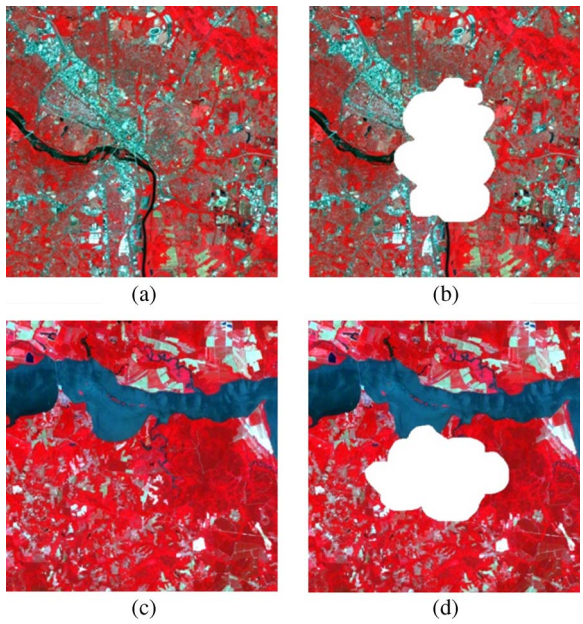


Fig. 3. NIR–red–green composites of Landsat ETM+ images acquired on July 4, 2002. (a) Heterogeneous subset. (c) Homogeneous subset. Figures (b) and (d) are the simulated cloudy images based on (a) and (c), respectively. The white area represents a simulated thick-cloud patch.

TABLE I
SUMMARY OF CLOUD SIZE (IN PIXELS) OF 100 SIMULATED CLOUDY IMAGES FOR EACH SUBSET

| Subset | Min | Max | Mean | Median |
|---|---|---|---|---|
| Heterogeneous | 1020 | 58542 | 21984 | 16978 |
| Homogeneous | 1467 | 48381 | 17310 | 13932 |

A Monte Carlo experiment was carried out to test the new method. For each subset image, 100 cloudy images were simulated based on the July 4 image. Specifically, to generate one cloudy image, a cloud patch with a random size (i.e., the number of pixels) was simulated at a random location on the July 4 image. The size of the simulated clouds varies according to a power law distribution [11]. In addition, given that the modified NSPI approach will use neighborhood information of clouds, the simulated clouds were rejected if they were located at the edge of the subset images. Fig. 3(b) and (d) shows an example of the simulated cloudy image for each subset. Table I summarizes the statistics of the simulated cloud size. For each subset, the images on January 25 and August 5 were used as the auxiliary images to remove the simulated clouds, respectively, which allowed us to evaluate the effect of temporal interval between the auxiliary image and the cloudy image.

Considering that real thick clouds are more complex than the simulated ones, a real cloudy Landsat 5 TM image (15 km × 15 km area in Ohio) acquired on July 24, 2008 [Fig. 4(a)], was also used to evaluate the modified NSPI

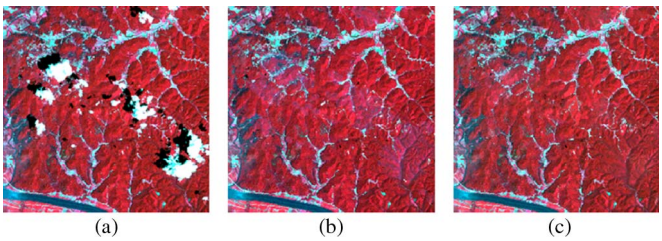


Fig. 4. (a) Landsat 5 TM image used in the real cloud-removal test. (b) Restored image from the CMLP approach. (c) Restored image from the modified NSPI approach.

method. Here, a cloud-free image acquired on June 6, 2008, was selected as an auxiliary image for thick-cloud removal.

For the purpose of comparison, CMLP was also applied to both simulated and real cloudy images to provide a benchmark to assess the strengths and limitations of the modified NSPI method, because CMLP was shown to be better than other cloud-removal methods [4]. Since both methods were applied to restore the same simulated cloudy images, the results of the two methods were not independent. Therefore, a paired Student $t$-test was used to determine if the difference between the two methods is statistically significant.

### B. Results of Simulated Clouds

The minimum number of similar pixels ($N$) is the only parameter to be set in the modified NSPI method. A trial-and-error procedure was used to calibrate parameter $N$ in this letter. Our results revealed that the reflectance prediction is more accurate when using a larger $N$, but prediction accuracy becomes stable when $N$ reaches 20. For computational efficiency, $N$ was set to be 20 in the algorithm tests.

Fig. 5 shows the cloud-removal results from the simulated cloudy images by using the cloud-free image on January 25. It is visually clear that the image restored by the modified NSPI approach has less edge effects [see Fig. 5 (c) and (f)] and is more similar to the actual image than the result from the CMLP approach. Table II lists RMSE values of the restored images for each subset and reports $p$-values of the paired Student $t$-test between the two methods. Generally, the performance of the modified NSPI approach is better than that of the CMLP approach with smaller RMSE values. The difference between the two approaches is statistically significant ($p < 0.05$) in all the cases. Moreover, there is a positive correlation ($n = 12$, $R^2 = 0.899$, and $p < 0.001$) between the improvement in accuracy (i.e., the difference of mean RMSE between the modified NSPI and CMLP) and the spectral difference between the auxiliary image and the cloudy image (Diff in Table II), suggesting that the modified NSPI approach performs much better than the CMLP approach when using a temporally farther auxiliary image. This is very important for thick-cloud removal because it is often difficult to find an auxiliary image that is temporally close to the cloudy image.

### C. Results of Real Cloudy Image

Fig. 4(b) and (c) shows the cloud-removal results of the real cloudy image from the CMLP and modified NSPI approaches, respectively. Both methods can recover most of the image features blocked by thick clouds and shadows. However, the image restored by CMLP shows obvious edge effects, whereas they are nearly invisible in the restored image by the modified NSPI approach.

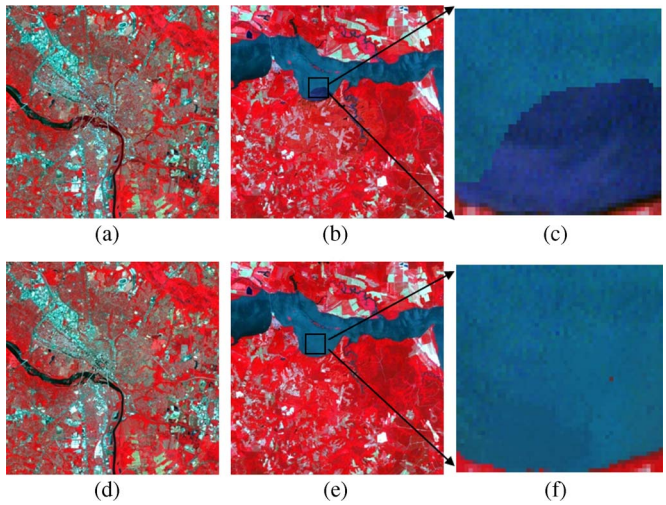


Fig. 5. Restored images for the simulated clouds in Fig. 3 by using the image on January 25. (a) and (b) By the CMLP approach. (d) and (e) By the modified NSPI approach. (c) and (f) Zoomed images of the area marked in (b) and (e), respectively.

TABLE II
MEAN AND STANDARD DEVIATION (SD) OF RMSE VALUES BY CMLP AND THE MODIFIED NSPI METHOD FOR SUBSET 1 (HETEROGENEOUS) AND SUBSET 2 (HOMOGENEOUS) FROM THE MONTE CARLO EXPERIMENT

| Subset | Auxiliary image | Band | CMLP Mean (SD) | NSPI Mean (SD) | Diff | *p*-value |
|---|---|---|---|---|---|---|
| 1 | 01/25 | Green | 0.0200(0.0044) | 0.0193(0.0042) | 0.0233 | <0.0001 |
| | | Red | 0.0306(0.0082) | 0.0280(0.0081) | 0.0344 | <0.0001 |
| | | NIR | 0.0543(0.0074) | 0.0429(0.0044) | 0.1679 | <0.0001 |
| | 08/05 | Green | 0.0099(0.0020) | 0.0097(0.0020) | 0.0103 | 0.0003 |
| | | Red | 0.0154(0.0058) | 0.0148(0.0058) | 0.0170 | 0.0002 |
| | | NIR | 0.0203(0.0059) | 0.0196(0.0046) | 0.0368 | 0.0004 |
| 2 | 01/25 | Green | 0.0113(0.0040) | 0.0102(0.0034) | 0.0146 | 0.0001 |
| | | Red | 0.0194(0.0060) | 0.0161(0.0055) | 0.0286 | <0.0001 |
| | | NIR | 0.0511(0.0091) | 0.0412(0.0096) | 0.1804 | <0.0001 |
| | 08/05 | Green | 0.0086(0.0025) | 0.0066(0.0020) | 0.0115 | <0.0001 |
| | | Red | 0.0134(0.0050) | 0.0105(0.0043) | 0.0186 | <0.0001 |
| | | NIR | 0.0248(0.0072) | 0.0236(0.0050) | 0.0471 | 0.0155 |

## IV. CONCLUSION AND DISCUSSION

In this letter, we have developed a modified NSPI approach for removing thick-cloud contamination on Landsat imagery. Compared with CMLP, the proposed method can restore an image with less edge effects. More importantly, the reflectance values estimated by the modified NSPI approach are more accurate than the results from CMLP when the cloud-free auxiliary image and the cloudy image are acquired from different seasons and have different spectral characteristics.

The improved performance of the new method can be ascribed to three aspects. First, similar pixels are used to provide

change information between the cloud-free image and the cloudy image, which can effectively account for the radiometric difference between two images. That is the reason why the modified NSPI approach is more effective when time interval between the auxiliary and the cloudy image is longer. This approach can also be applied to images at the digital number level over flat terrains, because the difference of illumination between two images can be taken into account by the change term in (2). For mountainous areas, topographic correction is needed before the cloud removal [12]. Second, the modified NSPI approach makes use of the spectral information in a sufficient number of similar pixels, which can guarantee its reliability from a statistical viewpoint. In contrast, the CSF method only uses the spectral-closest cloud-free pixel, and the CMLP method just utilizes the corresponding pixel from the cloud-free images as input of the contextual regression model to predict the value of cloudy pixel. Third, the weighted combination of two predictions ensures the spatial and radiometric continuity of the restored image according to the relative usefulness of spectro-spatial and spectro-temporal information.

There are some limitations about the modified NSPI approach. First, similar to CMLP [4], the accuracy of the recovered image slightly decreases with the increased cloud size. This may be because both methods use neighborhood information of clouds. As the cloud size increases, the average distance between a target pixel and its similar pixels increases and their correlation decreases, resulting in reduced prediction accuracy. Second, for regions with frequent presence of clouds, it is hard to obtain cloud-free auxiliary images from the same Landsat sensor. A recent study has shown the potential to build consistent time-series data from multiple Landsat-like resolution sensors using a reference-based approach [13]. The approach can provide an additional auxiliary clear image to choose from. We will explore the use of images from different sensors to remove cloud contamination in the future.

## REFERENCES

[1] J. C. Ju and D. P. Roy, "The availability of cloud-free Landsat ETM plus data over the conterminous United States and globally," *Remote Sens. Environ.*, vol. 112, pp. 1196–1211, 2008.

[2] E. H. Helmer and B. Ruefenacht, "Cloud-free satellite image mosaics with regression trees and histogram matching," *Photogramm. Eng. Remote Sens.*, vol. 71, no. 9, pp. 1079–1089, Sep. 2005.

[3] Q. M. Meng, B. E. Borders, C. J. Cieszewski, and M. Madden, "Closest spectral fit for removing clouds and cloud shadows," *Photogramm. Eng. Remote Sens.*, vol. 75, no. 5, pp. 569–576, May 2009.

[4] F. Melgani, "Contextual reconstruction of cloud-contaminated multitemporal multispectral images," *IEEE Trans. Geosci. Remote Sens.*, vol. 44, no. 2, pp. 442–455, Feb. 2006.

[5] S. Benabdelkader and F. Melgani, "Contextual spatiospectral postreconstruction of cloud-contaminated images," *IEEE Trans. Geosci. Remote Sens. Lett.*, vol. 5, no. 2, pp. 204–208, Apr. 2008.

[6] J. Chen, X. Zhu, J. E. Vogelmann, F. Gao, and S. Jin, "A simple and effective method for filling gaps in Landsat ETM+ SLC-off images," *Remote Sens. Environ.*, vol. 115, no. 4, pp. 1053–1064, Apr. 2011.

[7] H. Choi and R. Bindschadler, "Cloud detection in Landsat imagery of ice sheets using shadow matching technique and automatic normalized difference snow index threshold value decision," *Remote Sens. Environ.*, vol. 91, no. 2, pp. 237–242, May 2004.

[8] X. Zhu, J. Chen, F. Gao, and J. G. Masek, "An enhanced spatial and temporal adaptive reflectance fusion model for complex heterogeneous regions," *Remote Sens. Environ.*, vol. 114, no. 11, pp. 2610–2613, Nov. 2010.

[9] J. G. Masek, E. F. Vermote, N. E. Saleous, R. Wolfe, F. G. Hall, K. F. Huemmrich, F. Gao, J. Kutler, and T. K. Lim, "A Landsat surface reflectance dataset for North America, 1990–2000," *IEEE Geosci. Remote Sensing Letters*, vol. 3, no. 1, pp. 68–72, Jan. 2006.

[10] F. Gao, J. G. Masek, and R. E. Wolfe, "Automated registration and orthorectification package for Landsat and Landsat-like data processing," *J. Appl. Remote Sens.*, vol. 3, no. 1, p. 033 515 , Mar. 2009.

[11] R. A. J. Neggers, H. J. J. Jonker, and A. P. Siebesma, "Size statistics of cumulus cloud populations in large-eddy simulations," *J. Atmos. Sci.*, vol. 60, no. 8, pp. 1060–1074, Apr. 2003.

[12] D. Riano, E. Chuvieco, J. Salas, and I. Aguado, "Assessment of different topographic corrections in Landsat-TM data for mapping vegetation types," *IEEE Trans. Geosci. Remote Sens.*, vol. 41, no. 5, pp. 1056–1061, May 2003.

[13] F. Gao, J. G. Masek, R. Wolfe, and C. Huang, "Building consistent medium resolution satellite data set using moderate resolution imaging spectroradiometer products as reference," *J. Appl. Remote Sens.*, vol. 4, p. 043 526, Apr. 2010. DOI:10.1117/1.3430002.